THE ASTROPHYSICAL JOURNAL, 468:823–833, 1996 September 10

DELAYED COLLAPSE OF HOT NEUTRON STARS TO BLACK HOLES VIA HADRONIC PHASE TRANSITIONS

THOMAS W. BAUMGARTE
Center for Radiophysics and Space Research, Cornell University, Ithaca, NY 14853; baumgart@astrosun.tn.cornell.edu

H.-THOMAS JANKA[1] AND WOLFGANG KEIL
Max-Planck-Institut für Astrophysik, Karl-Schwarzschild-Straße 1, 85740 Garching, Germany;
thj@mpa-garching.mpg.de, wfk@mpa-garching.mpg.de

STUART L. SHAPIRO
Center for Astrophysics and Relativity, 326 Siena Drive, Ithaca, NY 14850; shapiro@astrosun.tn.cornell.edu

AND

SAUL A. TEUKOLSKY[2]
Center for Radiophysics and Space Research, Cornell University, Ithaca, NY 14853; saul@astrosun.tn.cornell.edu
Received 1995 December 8; accepted 1996 April 4

ABSTRACT

We present numerical simulations of the delayed collapse of a hot nascent neutron star to a black hole. Using a recently developed, singularity-avoiding dynamical code we can follow the collapse to completion and can study the late-time effects. We employ a hyperonic equation of state which is softer for deleptonized matter than for lepton-rich matter. For this equation of state the maximum mass of stable neutron stars therefore decreases as the protoneutron star loses lepton number by emission of electron neutrinos during the first seconds after its formation in the core bounce in a supernova. Protoneutron stars with masses within a critical window are therefore stable initially but later inevitably collapse to a black hole.

We study the last stages before such a collapse, as well as the final, dynamical implosion, tracking the evolution of the star until its surface reaches the event horizon. In particular, we determine the characteristics of the neutrino emission during this delayed collapse of the protoneutron star. Since hot neutron star matter is opaque to neutrinos, we find that there is no late increase or final, powerful outburst of the neutrino emission. Instead, the fluxes gradually decrease as more and more matter in the star approaches the event horizon and the gravitational redshift becomes extremely strong. Because muon and tau neutrinos as well as electron antineutrinos decouple from deeper, hotter layers than electron neutrinos, they are usually emitted with higher mean energies. During the last millisecond before the neutron star goes into the black hole, however, the gravitational redshift is so strong that the usual order of mean neutrino energies and fluxes is inverted.

Subject headings: black hole physics — dense matter — equation of state — methods: numerical — stars: evolution — stars: neutron

1. INTRODUCTION

The observation of neutrinos from SN 1987A (Alexeyev et al. 1987; Bionta et al. 1987; Hirata et al. 1987) confirmed the formation of a compact object capable of emitting neutrinos for a period of several seconds. The temporal correlation with the first optical sighting of SN 1987A (Shelton 1987) and the very good agreement of the properties of the neutrino burst (mean neutrino energies, total energy of the signal, duration of the burst) with theoretical predictions leave no doubt that SN 1987A was the source of the detected neutrinos, although some peculiarities in the measured data (time gap of about 7 s in Kamiokande, forward-peaked angular distributions of the events) might require further clarification.

In spite of the evidence that a protoneutron star was formed in SN 1987A, there has been no further indication of its existence. Excess radiation or even a pulsed signal that might be interpreted as evidence for a neutron star at the center of the supernova has not been observed (see, e.g., Percival et al. 1995). This lack of pulsar activity or emission from neutron star accretion has inspired speculations about the possible formation of a black hole in SN 1987A (Brown, Bruenn, & Wheeler 1992). From simple Bondi-Hoyle accretion models Brown & Weingartner (1994) concluded that the accretion luminosity of a neutron star should be well above current observational limits, whereas an accreting black hole would be invisible and hidden from detection. However, Colpi, Shapiro, & Wasserman (1995) have recently performed detailed calculations of spherical accretion in a uniformly expanding medium. They find that the accretion rate depends critically on the sound speed of the material at the onset of infall, and that the rate could be small enough that a neutron star could lie at the center of SN 1987A and remain undetected. Moreover, Chen & Colgate (1995) have argued that the absorption opacity of neutral or partially ionized iron is orders of magnitude higher than the Compton scattering opacity, thus reducing the Eddington limit of an accreting neutron star by a corresponding factor. They concluded that no revealing signature of accretion luminosity should be expected and even

[1] A portion of this work was carried out while on leave at the Department of Astronomy and Astrophysics, University of Chicago, Chicago, IL 60637.

[2] Departments of Astronomy and Physics, Cornell University, Ithaca, NY 14853.

the thermal X-ray emission of a hot young neutron star can still be obscured by the optically thick surrounding matter.

The formation of a black hole at the center of SN 1987A remains an interesting possibility that deserves further investigation. However, from the duration of the SN 1987A neutrino burst (~ 12 s) one must conclude that the collapse to the black hole can neither have happened promptly following the collapse of the stellar iron core nor following the postbounce accretion onto the collapsed core. The former scenario is expected when a stellar iron core undergoes gravitational collapse but is too massive to be stabilized even when the equation of state (EOS) stiffens at nuclear densities. Although very little is known about the character of the neutrino emission from such "prompt collapse," it is plausible that the neutrino signal is significantly different from the standard core collapse case and not consistent with the observations. Burrows (1988) investigated the accretion-induced instability initiated when enough matter has fallen onto the newly formed neutron star to push its mass over the cold stability limit. He found a powerful, but short ($\lesssim 2$s) neutrino pulse, with properties not compatible with the observational data from SN 1987A.

The collapse of the neutron star to a black hole might also be triggered by a sufficiently massive, late fallback of matter toward the neutron star. Recently, Woosley & Weaver (1995) modeled piston-driven explosions for a large number of progenitor stars and studied the development of reverse shocks and their implications for the fallback of matter to the neutron star. They found that the fallback happens at late times, i.e., after minutes to hours, providing ample time for the protoneutron star to lose its gravitational binding energy by the emission of neutrinos. For stellar models considered typical of the progenitor of SN 1987A, however, their results indicate that the amount of inward accelerated material might suffice to push the neutron star above the stability limit only if its mass was already very close to the maximum stable mass. (For a discussion of some aspects of accretion-induced neutron star collapse and the neutrino and photon emission of accreting neutron stars and black holes, see the recent papers by Fryer, Benz, & Herant 1996, Chen & Colgate 1995, and Colpi et al. 1995).

An exciting possibility that deserves further investigation is the delayed formation of a black hole caused by evolutionary changes of the neutron star EOS, such as a phase transition at supranuclear densities due to the formation of additional hadronic degrees of freedom besides neutrons and protons. While the neutron star is initially stable, the final gravitational instability could be a consequence of a softening of the EOS and a corresponding reduction of the maximum mass of stable configurations. Accretion would not play a crucial role. If the phase transition is triggered by the loss of energy or lepton number, it will naturally take place after a rather extended phase of neutrino emission. As long as the EOS is still stiff, the mass limit of stable stars can be above the initial protoneutron star mass, but might drop below it when the properties of the EOS have changed sufficiently. Brown & Bethe (1994) have discussed such "delayed collapse" as a consequence of the formation of a kaon condensate in the protoneutron star core. Baumgarte, Shapiro, & Teukolsky (1996, hereafter BST2) performed, with various simplifying assumptions, dynamical collapse calculations of this scenario in full general relativity. Keil & Janka (1995, hereafter KJ) have investigated the quasi-static, neutrino-driven evolution of the protoneutron star with a hyperonic EOS developed by Glendenning (1985; see also Glendenning 1995). In their simulations the phase transition and softening of the EOS were associated with the creation of hyperons, which is favored when the deleptonization of the star progresses and the neutron abundance increases. In principle, the formation of pions or pion condensates (Takahara, Takatsuka, & Sato 1991; Takatsuka 1992) can have similar effects. The crucial physical process for these delayed scenarios is a softening of the supranuclear EOS and a corresponding decrease of the upper mass limit of stable neutron stars.

The present paper reports simulations that represent a continuation and extension of the KJ work. KJ used a code that integrates the equations of hydrostatic stellar structure which is adequate to simulate the quasi-static Kelvin-Helmholtz neutrino-cooling phase of a nascent neutron star. Therefore KJ were not able to detect the final gravitational instability precisely nor were they able to follow the dynamical implosion of the neutron star to a black hole. The aim of the work presented here is to investigate in detail the approach to the instability and the final gravitational collapse of the hot protoneutron star to a black hole. We are primarily interested in a qualitative understanding of the astrophysical processes rather than quantitative precision. Nevertheless, we can follow the dynamical onset of instability and the formation of the black hole to completion. To do so we employ a hydrodynamical scheme recently developed by Baumgarte, Shapiro, & Teukolsky (1995, hereafter BST1) and used by BST2 with simplified microphysics for kaon condensation. This code solves the general relativistic equations using a coordinate system that avoids both coordinate and spacetime singularities (observer time coordinates). In § 2 properties of the numerical scheme will be summarized, the treatment of the neutrino physics and the properties of the adopted EOS will be described, and our initial model and the relationship to the earlier KJ work will be detailed. Section 3 deals with the results of our simulations of neutron star collapse and black hole formation, and § 4 concludes with a discussion and final remarks.

2. SETUP OF THE PROBLEM

Most of the ingredients in our calculations have already been described elsewhere. Except for the parts original to this work we will therefore sketch the main ideas only and refer the reader to the literature for more details.

2.1. *The Numerical Scheme*

We use a finite-difference scheme to solve the fully relativistic, Lagrangian equations of hydrodynamics in spherical symmetry. The code has been developed and tested in BST1, to which the reader is referred for a detailed description.

The virtue of this scheme is the use of a retarded time u, which is constant along outgoing light rays and agrees with the proper time of a stationary observer at infinity ("observer time coordinates"; Hernandez & Misner 1966). By definition, an outward light ray emitted from inside a black hole will never reach infinity; for this reason no event inside a black hole corresponds to a finite observer time u. Our coordinate system therefore covers the complete spacetime outside the event horizon, but never penetrates inside a black hole that may form. We can thus follow the collapse

to a black hole to completion without ever encountering a singularity. In particular, we can calculate the neutrino signal even from the very late stages of such a collapse.

In addition to the observer time u we use the enclosed rest mass A as a (comoving) radial coordinate. Since our code is explicit, the time steps are restricted by a Courant condition. Therefore it requires an appreciable number of time steps to perform computations over evolution periods of about 100 ms. Also, both the evaluation of the equation of state (EOS) (§ 2.3) and the neutrino leakage scheme (§ 2.2) require appreciable computing time. We have therefore limited our simulation to 30 radial grid points which are equally spaced in A.

The hot protoneutron star is still very opaque to neutrinos (except for the outermost layer). The neutrino luminosities in this problem are very small compared to the Eddington luminosity, and neutrinos contribute only an insignificant fraction to the total pressure and energy density. For these reasons we can safely approximate the neutrino pressure and energy density by assuming local thermodynamic equilibrium between neutrinos and the stellar gas everywhere in the star. The neutrino contributions are added to the total pressure and internal energy of the nuclear EOS (see KJ for more details). We neglect neutrino radiation terms in all hydrodynamical equations except for the equation of local energy conservation, where we include an effective energy source/sink term due to neutrino emission. Therefore the hydrodynamics code presented in BST1 can be used with only minor changes. Apart from implementing the EOS (§ 2.3) we have to add the electron number fraction $Y_e = n_e/n$ as a new variable and a corresponding evolution equation where, again, neutrino losses provide a source term. Here n is the baryon number density, and $n_e = n_{e^-} - n_{e^+}$ is the net electron number density.

Once per time step the program calls the "leakage scheme" (§ 2.2), which returns an effective energy loss rate $Q^{\rm eff}$ (per unit mass) and an effective deleptonization rate $S^{\rm eff}$ (per nucleon) due to the neutrino emission. The former is added as a source term in the energy equation (first law of thermodynamics),

$$\frac{\partial e}{\partial u} = -P \frac{\partial}{\partial u}\left(\frac{1}{\rho_0}\right) + e^{\psi} Q^{\rm eff} . \tag{1}$$

Here e is the specific internal energy, P is the total pressure (including contributions from nucleons, electrons, positrons, radiation, and neutrinos in equilibrium with the gas), $\rho_0 = nm_u$ is the rest mass density (where we use $m_u = 1.66 \times 10^{-24}$ g as atomic mass unit), and e^{ψ} is the lapse function. Note that $\partial/\partial u$ denotes the Lagrangian time derivative. Equation (1) replaces equation (39) in BST1. In each time step the update of the electron number fraction is done according to

$$\frac{\partial Y_e}{\partial u} = e^{\psi} S^{\rm eff} . \tag{2}$$

This equation has to be added to the evolution scheme in BST1. The treatment of the neutrino physics is described in the following section. Details about the source terms $Q^{\rm eff}$ and $S^{\rm eff}$ can be found in Appendix B of Ruffert, Janka, & Schäfer (1996), in particular in equations (B24) and (B25) where $\rho_0 Q^{\rm eff}$ is denoted by Q_ϵ^- and $nS^{\rm eff}$ by $R_{Y_e}^-$. Since these terms give the rates with respect to proper time τ of a comoving observer and not with respect to observer time u, they have to be multiplied by $d\tau/du = e^{\psi}$ in equations (1) and (2).

2.2. *Treatment of Neutrinos*

Before the start of our simulations, the protoneutron star has undergone about 10 s of deleptonization and cooling by neutrino emission. By the time the gravitational instability is triggered, the lepton number and energy fluxes are directed outward in the whole star. In the present work we simulate only the very last stages of the protoneutron star evolution before its final collapse, i.e., a total period of only about 100 ms, which is short relative to the neutrino diffusion timescale ($\gtrsim 1$ s). Therefore the transport of neutrinos inside the star and the associated transfer of lepton number and energy are of minor importance compared to the overall net energy loss and the global shift of the composition by the emission of neutrinos. In fact, the ongoing deleptonization drives the gradual hyperonization and finally leads to the gravitational instability. This is not much affected by details of differential changes of composition and temperature during the precollapse phase. Thus it is a viable approximation to treat the neutrino effects with a leakage scheme.

In contrast to a transport description like, for example, diffusion, a leakage scheme only estimates the local net loss of lepton number and energy for every grid point. The total loss rates are then found by summing over all grid points. The leakage scheme used in the present hydrodynamical models is described in Ruffert et al. (1996), where expressions for the relevant neutrino production rates and for the neutrino opacities also can be found.

Neutrinos of all three types are created by electron-positron pair annihilation

$$e^- + e^+ \rightarrow \nu_i + \bar{\nu}_i , \tag{3}$$

and by plasmon decay

$$\tilde{\gamma} \rightarrow \nu_i + \bar{\nu}_i , \tag{4}$$

which dominates at high densities and high electron degeneracies. Additionally, electron-type neutrinos are created via charged-current β-processes

$$\begin{aligned} e^- + p &\rightarrow n + \nu_e , \\ e^+ + n &\rightarrow p + \bar{\nu}_e . \end{aligned} \tag{5}$$

While the emission of ν_e and $\bar{\nu}_e$ changes the electron number fraction Y_e in addition to extracting energy, the heavy-lepton neutrinos ν_μ, $\bar{\nu}_\mu$, ν_τ and $\bar{\nu}_\tau$ only carry away energy. Since their transport is very similar, they are treated like one species ν_x with a statistical weight of 4.

At low optical depths, the production and emission of neutrinos is computed directly from the rates of the above processes. At high optical depths neutrinos are assumed to be present in their chemical equilibrium abundances, and the loss of neutrino number and energy proceeds on the local diffusion timescale rather than on the neutrino production timescale. An appropriate interpolation between the two extreme cases yields the effective local energy loss rate $Q^{\rm eff}$ and the deleptonization rate $S^{\rm eff}$. Adding the properly redshifted emission from all zones of the grid gives the star's neutrino luminosities for a stationary observer at infinity, $e^{2\psi} L_{\nu_i}$, and the corresponding total neutrino number fluxes. The mean energies of the emitted neutrinos can be calculated as the ratio of energy and number fluxes.

For the calculation of the optical depths and the diffusion timescales both neutral-current scattering off nucleons and, for the electron-type neutrinos, the inverse β-processes are taken into account. All radial integrals are carried out over proper radius in order to account for relativistic length contraction.

In the leakage scheme the lepton number source term and the energy source term are computed separately because they differ in the energy moments (integrals) of the phase space distributions of the reacting fermions. Besides the freedom associated with the decoupled handling of lepton and energy sectors, another free parameter exists in a numerical factor that relates the local diffusion timescale with the radial position inside the star (see Ruffert et al. 1996). These free parameters were exploited to calibrate the leakage scheme to yield lepton number loss rates very similar to those obtained in the neutrino diffusion treatment of KJ. However, at low optical depths the leakage scheme used here explicitly evaluates the neutrino losses from the reaction rates, while the transport approximation employed by KJ was a flux-limited equilibrium-diffusion method that assumed neutrinos to be present in their chemical equilibrium distributions even in the layers close to the surface of the star. There the offstreaming of neutrinos and thus the evolutionary shift of β-equilibrium were influenced by the use of the flux limiter. Although the calibration of our leakage scheme attempts to reduce the discrepancies of both descriptions to a minimum, the technical differences of both methods lead to an unavoidable relaxation phase when our simulations are started from initial data provided from one of the KJ models (§ 2.4). The values to which the stellar profiles like Y_e and T relax are only slightly different from the KJ model, and the neutrino luminosities and mean energies of neutrinos emitted after the first $\sim$40 ms are in very good agreement with the results of the diffusion method of KJ.

2.3. *Equation of State*

At the densities present in the cores of neutron stars, the Fermi momenta of the nucleons are high enough that additional hadronic states besides the neutron and proton might occur. While there is wide agreement about this possibility in principle, it remains unclear which new particles are the most favored ones. In this paper we adopt an EOS where the ground state is attained by a mixture of neutrons, protons, hyperons, and Δ-resonances in the hadronic sector, and electrons and muons in the leptonic sector (Glendenning 1985). In neutronized matter the most important reaction for the creation of hyperons ($\Lambda, \Sigma, \Xi, \ldots$) is

$$n + n \rightarrow n + \Lambda + K \, . \qquad (6)$$

The adopted EOS is different from those proposed by Thorsson, Prakash, & Lattimer (1994) and Brown & Bethe (1994) in that the kaons cannot form a condensate but instead decay into photons, muons, and neutrinos. The Λ-particles, however, are Pauli blocked and do not decay. According to Glendenning (1985) they may therefore represent up to 20% of the total baryon population in the cores of massive neutron stars. Mayle, Tavani, & Wilson (1993) considered the presence of pions in the supernova core, but in their EOS no pion condensate forms. Some groups (Takahara et al. 1991; Takatsuka 1992), on the other hand, did study the occurrence of pion condensates at supranuclear densities.

Since Λ-particles have a higher effective mass in dense matter than neutrons, the creation of these new hadronic states requires energy from the reservoirs of thermal and degeneracy energy. Also, because of the availability of new degrees of freedom, the neutron density and the Fermi energy of the neutrons are reduced. Correspondingly, the pressure becomes smaller for the same value of density, and the EOS softens, i.e., the increase of the pressure with density becomes less steep (see Fig. 1 in KJ). This effect sets in at a critical density of about $\rho_{\rm hyp} = 5 \times 10^{14}$ g cm^{-3} (baryon density $n \approx 0.3$ fm^{-3}, roughly twice nuclear matter density) and is stronger when the neutron abundance is high.

The softening of the supranuclear EOS, triggered by the formation of hyperons when the matter of the newly formed neutron star deleptonizes, has important and very interesting astrophysical consequences. The maximum mass of neutron stars with a high lepton ($n_{e^-} - n_{e^+} + n_{\nu_e} - n_{\bar{\nu}_e}$) concentration is larger than the maximum mass for deleptonized stars. A (cold) star with $Y_{\rm lep} = 0.3$ is stable for a gravitational mass up to $M_{\rm max} = 1.77\ M_\odot$ (corresponding to a baryonic mass of $1.94\ M_\odot$), while the maximum mass for a deleptonized (cold) star is $1.58\ M_\odot$ (baryonic mass $1.77\ M_\odot$). A newly formed and still lepton-rich neutron star in this mass window will therefore be initially stable. However, as the deleptonization proceeds through the emission of electron neutrinos, more and more hyperons are formed via processes like that in equation (6), and the EOS softens. This gradually reduces the mass limit for stability, and eventually the star will trigger gravitational instability and collapse on a dynamical timescale. If no other more tightly bound and less energetic state of the matter is encountered (e.g., a quark plasma) where the EOS stiffens again, this collapse will inevitably lead to a black hole. An important consequence is therefore that stellar collapse can produce both a supernova and a black hole. It is on this delayed collapse that we will focus in this paper.

Further information about the physical input into the EOS and its properties can be found in Glendenning (1985, 1989). The extension of Glendenning's $T = 0$ EOS with temperature corrections and the numerical handling of our EOS were detailed in KJ, and various astrophysical implications were discussed by Glendenning (1985), KJ, Janka (1995), and Glendenning (1995).

2.4. *The Initial Model*

Our initial data are taken from model LBH in KJ, which has a baryonic mass of $A_{\rm tot} = 1.78\ M_\odot$, only slightly above the stability limit of the adopted hyperonic EOS. We start our simulations at a stage shortly before the model reached the onset of gravitational instability in the KJ simulation. The dynamical collapse was found to occur at about 9.6s after the start of the computation or roughly 10.2 s after stellar core bounce and the formation of the protoneutron star. The initial model for the simulation presented here is taken at about 9.2 s. At this time the gravitational mass of the still very hot nascent neutron star (central temperature around 60 MeV) is $M = 1.65\ M_\odot$, which is considerably larger than the stability limit of $1.58\ M_\odot$ for the cold, deleptonized state. The neutrino-driven evolution preceding our initial model was described in detail in KJ, where the predicted signal in neutrino experiments was also analyzed, and a comparison of model LBH with a sample of other protoneutron star cooling models with different masses,

initial temperatures, and equations of state was presented. At the moment when model LBH tends to become dynamically unstable, it is not yet completely deleptonized, and neutronization and the resulting hyperonization in its high-density interior core are still progressing. This allows us to follow closely the changes of the stellar structure in response to the softening of the EOS shortly before and during the dynamical phase of the gravitational collapse.

The dynamical code employed here and the scheme used by KJ are not completely compatible. The simulations of KJ were performed with a Henyey-type stellar evolution code which iteratively evolves the equations for hydrostatic stellar structure and neutrino diffusion. This approximation implies that dynamical terms are neglected, and that the star is forced into hydrostatic equilibrium. KJ had to stop their calculations at the onset of the gravitational instability when the changes in the star became so fast that the code no longer yielded converged solutions. Since hydrostatic equilibrium is an artificially imposed constraint on the proto-neutron star evolution, the KJ simulations do not determine the moment of the onset of the gravitational instability very precisely. It is likely that their simulation overestimated the duration of the quasi-static evolution of the protoneutron star. The time from which data of their simulation are taken as an input to begin the dynamical calculations has therefore to be chosen very carefully. By starting the dynamical integrations from KJ models for different times, while the neutrino emission was switched off, we could determine whether a particular model was already unstable or still stable against radial perturbations. With 30 grid points the dynamical code locates the moment of dynamical instability about 0.3–0.4 s earlier than found by KJ. For the calculation described in § 3 we use KJ data after an evolution time of 9.168s. Our tests made sure that the subsequent collapse of this model is triggered by the deleptonization and the hyperonic phase transition in the EOS. Collapse is caused by the physical evolution from an initially stable state.

With only 30 grid points the numerically determined time for the onset of the instability in the model can only be taken as an estimate. The actual time of the instability would have to be determined with a very high-resolution run and might occur even slightly earlier than found in the low-resolution runs. However, in this paper our goal is qualitative insight rather than quantitative precision, for which 30 grid points proved to be sufficient. As a measure of error the total energy was conserved up to about 1%.

The different discretization in the dynamical simulations and therefore different representation of the pressure gradients compared to KJ has also another consequence. The initial model, mapped onto our grid, is not exactly in hydrostatic equilibrium and starts a small-amplitude, radial pulsation with a typical period of 2ms (observer time), corresponding to the fundamental pulsation mode of the neutron star. Depending on the details of the numerical treatment (which determines the intrinsic, numerical viscosity of the code) this oscillation can be damped out very quickly (as in the run described in § 3), or can continue for a rather long time and for many cycles. We found both kinds of behavior in the set of test runs that we performed with varied grid resolution and neutrino description. In neither case was the global evolution affected or changed by the presence, absence, or degree of damping of these initial pulsations and the associated dynamical relaxation.

As already discussed in § 2.2, the switching from the neutrino description applied by KJ to the leakage scheme used in this work also implied a thermodynamical relaxation of the model. Slight changes of the temperature, electron fraction Y_e, and electron and electron neutrino chemical potentials, μ_e and μ_{ν_e}, in the outermost $\sim 0.5\ M_\odot$ during the first ~ 40–50 ms of our simulations reflect the adjustment of the model. Although free parameters and remaining degrees of freedom in the leakage scheme were calibrated to minimize these effects, the initial shifts of temperature and composition particularly affect the electron neutrino luminosity, which starts out from an artificially high value. After the relaxation of the temperature and Y_e profiles in the star, however, the electron neutrino flux also settles to a quasi-stationary, slowly decaying value and evolves coherently with the luminosities of the other neutrino types. Again, the phases of the protoneutron star evolution that are most interesting for the present work are not disturbed by this relaxation. This was tested by making modifications in the settings of the free parameters in the leakage scheme and performing comparative runs. While the electron neutrino flux and the total evolution time to the final gravitational instability were somewhat sensitive to these manipulations, the average energy of the emitted ν_e showed a minor dependence, and the overall temporal behavior and evolution of the model as well as the $\bar{\nu}_e$ and ν_x luminosities and mean energies were insensitive to the differences of the numerics in the various test runs.

3. RESULTS

In this section we present the results of a dynamical calculation which simulates the cooling and deleptonization of the hot protoneutron star for a period of about 125 ms, beginning from an initial state at about 10 s after core bounce (§ 2.4), through the onset of the gravitational instability, until the moment when the surface reaches the event horizon. The evolution can be divided into three distinct phases. The first 40–50 ms are characterized by a dynamical and thermodynamical relaxation process which is a numerical artifact and simply caused by the settling of the initial data taken from the model of KJ (see § 2.4). Numerical relaxation is then followed by a quasi-static, very slow contraction of the protoneutron star for more than 70 ms. It is driven primarily by the loss of lepton number via emission of electron neutrinos and the associated advancing hyperonization of the protoneutron stellar matter. Finally, between 120 and 125 ms after the start of the simulation, the EOS has softened so much that the gravitational instability is encountered and the dynamical collapse of the star into a black hole begins. In calculations without neutrino loss the protoneutron star remains stable against radial perturbations and does not collapse.

3.1. *Evolution of the Stellar Structure*

Figure 1 shows the spacetime diagram of the neutrino-driven evolution. While the initial relaxation is barely visible in this diagram because it is associated only with minor rather fast adjustments of the stellar radius and the stellar density profile, the long quasi-static phase and the subsequent, short dynamical collapse can clearly be identified. During the quasi-static period one can notice a slow but steady contraction of the whole star. The stellar radius shrinks by about 200–250 m until $u = 120.0$ ms. Between $u = 120.0$ ms and $u = 125.0$ ms the evolution speeds up, and the star contracts by a similar

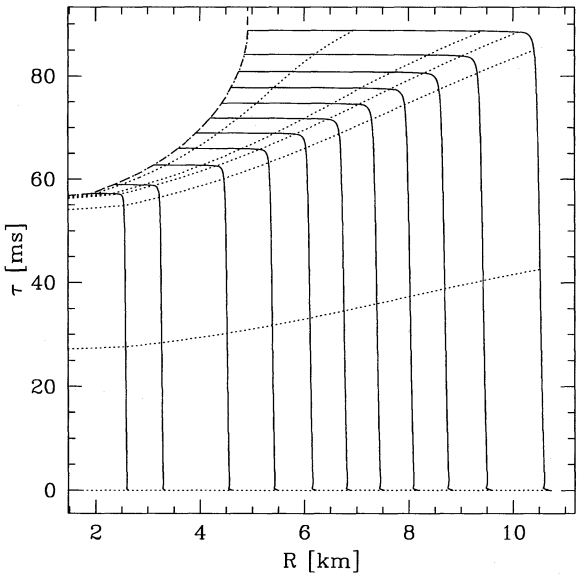

FIG. 1.—Spacetime diagram of the delayed collapse. The worldlines of representative fluid mass shells (*solid lines*) are plotted in terms of proper time τ vs. a real radius R. The event horizon is given by the dashed line. The dotted curves mark lines of constant observer time u for $u = 0$, 60.0, 120.0, 125.0, 125.3, 125.5, and 125.7 ms, respectively. The $u = 125.7$ ms line essentially coincides with the event horizon.

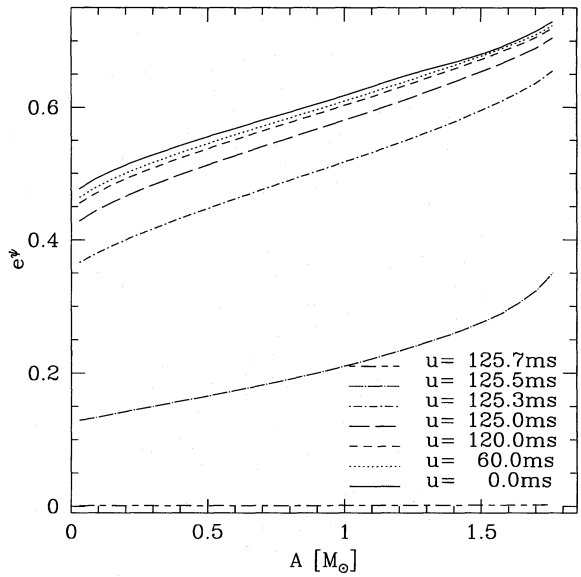

FIG. 2.—Radial profiles of the lapse function e^{ψ} for different observer times u. The radial position is expressed in terms of the enclosed rest (baryonic) mass A of the star which is measured in units of the solar mass. Because of the monotonic contraction of the star the lapse function decreases continuously.

amount as it did during the entire preceding 120 ms. Finally, the changes become extremely fast when the dynamical collapse sets in ($u \gtrsim 125.0$ ms). For an observer at infinity, the dynamical infall happens within less than 1ms. At times $u \gtrsim 125.0$ ms the whole star is "seen" in the state of dynamical contraction; at $u \approx 125.7$ ms even the surface layers have already reached the event horizon. In Figure 1 it looks like the core collapses about 32 ms earlier than the surface of the star. This is because we have plotted the proper time τ for each individual mass shell. We consider the collapse as completed when e^{ψ} has decreased to extremely small values in the whole star.

The lapse function e^{ψ}, displayed in Figure 2 as a function of the enclosed rest mass A at different observer times u, decreases only little in the first 120 ms. This is correlated with the slight contraction of the star during the quasi-static period as seen in Figure 1. At late times during the dynamical phase of the collapse e^{ψ} rapidly shrinks to vanishingly small values as the event horizon is approached (Fig. 1). We stopped our calculation when e^{ψ} for the outermost mass shell had become less than 10^{-5}. This is the case at $u = 125.9$ ms. Due to the small values of e^{ψ} the collapse is "frozen in" at that time, i.e., the radial profile of the infall velocity, the stellar structure, and the thermodynamical parameters exhibit essentially no change with u any more.

In Figure 3 we show profiles of the coordinate velocity U. In the quasi-static phase the contraction is slow so that up to $u = 125.0$ ms the velocities remain very small, even during an initial oscillation induced by the out-of-equilibrium initial configuration (see § 2.4). Dynamical effects become important only after 125.0 ms. The peak values of the velocity during the collapse are close to $0.5c$ and are found in the surface layers when these cross the event horizon at $u > 125.7$ ms. In the subsequent evolution, between 125.7 ms and the end of our simulation at 125.9 ms, the values of U are nearly identical, and we therefore did not include a later time in Figure 3. The last profile for $u = 125.7$ ms essentially lies on the event horizon.

While the velocities for $u < 125.0$ ms are small, the star nevertheless contracts. This is clearly visible in Figure 4, where the profile of the rest mass density ρ_0 is plotted for different times u, and in Figure 5, which gives the corresponding temperature distributions. Density as well as temperature increase during the quasi-static contraction, the latter primarily due to compressional heating. The moderate shrinking of the stellar radius by about 200–250 m in the first 120 ms, corresponding to a relative change by roughly 2%–2.5%, is accompanied by an increase of the central density by about 8%–9% from 1.60×10^{15} g cm^{-3} to

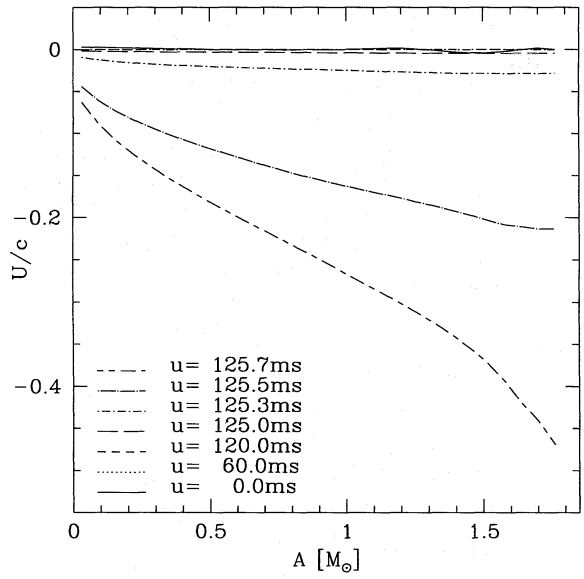

FIG. 3.—Radial profiles of the coordinate velocity U for different observer times u. At late times the infall velocity reaches a significant fraction of the speed of light.

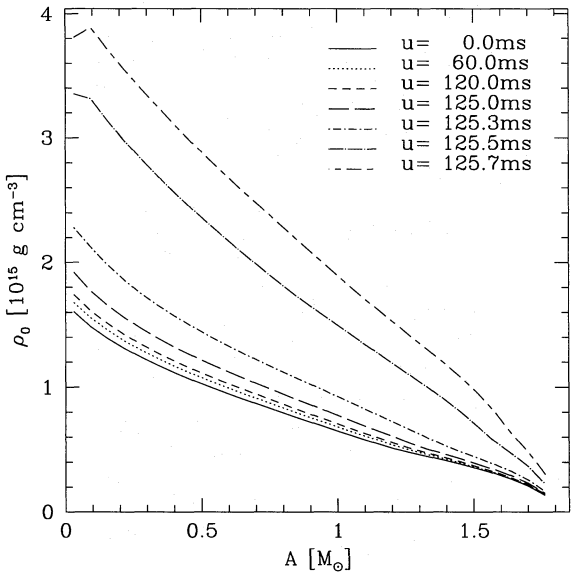

FIG. 4.—Radial profiles of the rest mass density ρ_0 for different observer times u. The monotonic contraction of the star implies a continuous increase of ρ_0.

1.74×10^{15} g cm^{-3}. The initial central temperature of ~ 60 MeV increases by 2.5 MeV or 4% during this time. The strong compression in the final, dynamical collapse pushes the central temperature to a maximum value of nearly 100 MeV and the central density to a peak value of 4×10^{15} g cm^{-3} which is reached at the moment when the surface approaches the event horizon. At the same time the density in the outermost layers has increased by roughly a factor of 2 compared with the initial state, when it was $\sim 1.4 \times 10^{14}$ g cm^{-3}, and the surface temperature has climbed from about 8 MeV to 12 MeV. Note that during the early relaxation ($u \lesssim 50$ ms), the temperature at the surface drops from 10 MeV initially to only 8 MeV due to neutrino emission, and the protoneutron star becomes cooler in the outermost ~ 0.3–$0.4\ M_\odot$ for an intermediate phase of the evolution.

Hyperonization occurs above a density of about 5×10^{14} g cm^{-3} and is favored by strong nucleon degeneracy. It affects an increasingly larger fraction of the interior as the deleptonization progresses via the emission of electron neutrinos and as the interior density increases with the stellar contraction. The mass shell interior to which hyperon production takes place moves out from $A \approx 1.2$–$1.3\ M_\odot$ initially to $A \approx 1.6$–$1.7\ M_\odot$ at $u = 125.7$ ms. Hyperonization softens the EOS, thus causes a further shrinking of the star and a further density increase, which, again, allows the phase transition to become more prominent. At some stage stability can no longer be maintained, and the contraction accelerates via dynamical collapse.

Figure 6 displays the evolution of the electron fraction Y_e, which reflects the effects of the electron neutrino and antineutrino emission. Y_e decreases in the high-density interior region ($A \lesssim 1.2\ M_\odot$) which is most crucial for the stability of the star because there the hyperonization is strongest. In the outer $\sim 0.5\ M_\odot$ the electron abundance slowly increases during the whole evolution which means that the matter emits more electron antineutrinos than electron neutrinos. This is a consequence of the shift of β-equilibrium in response to the contraction of the star. As the density in the star increases, the chemical potentials of nucleons (nonrelativistic) and leptons (relativistic) grow by different amounts, leading to a shift of the balance of the β-processes, equation (5), and their inverse reactions. This can be seen in Figure 7, where the chemical potentials (Fermi energies) of electron neutrinos, $\mu_{\nu_e} = \mu_e + \mu_p - \mu_n$, are given at different times u. Although still rather close to zero in the outer part of the star (where the densities are lower than $\rho_{\rm hyp}$), one can notice a slight shift of μ_{ν_e} to the negative side. This becomes particularly apparent during the very strong and fast compression in the dynamical collapse, when μ_{ν_e} drops to values as low as -35 MeV in the outermost 0.2–0.3 $M_\odot$. Since the neutrino-driven evolution of the protoneutron star tends to a state with $\mu_{\nu_e} = 0$, a shift of μ_{ν_e} toward negative values is

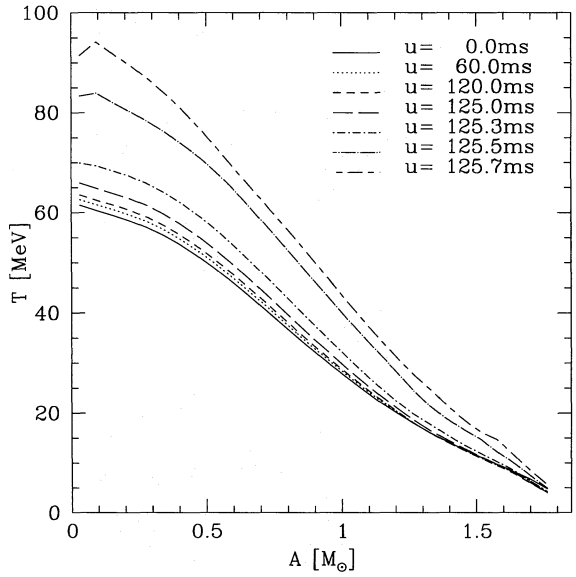

FIG. 5.—Radial profiles of the temperature T for different observer times u. Initially the temperatures decrease in the outermost ~ 0.3–$0.4\ M_\odot$ before the monotonic contraction of the star leads to rising temperatures in the whole star.

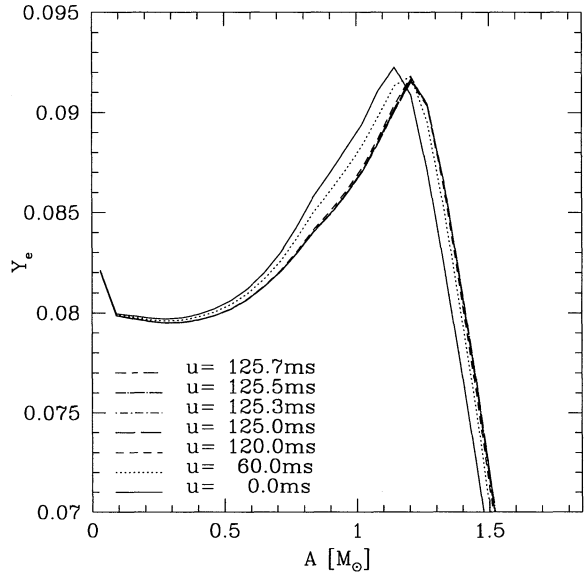

FIG. 6.—Radial profiles of the electron number fraction Y_e for different observer times u. The tiny decrease in Y_e near $A \sim 1\ M_\odot$ is responsible for the collapse.

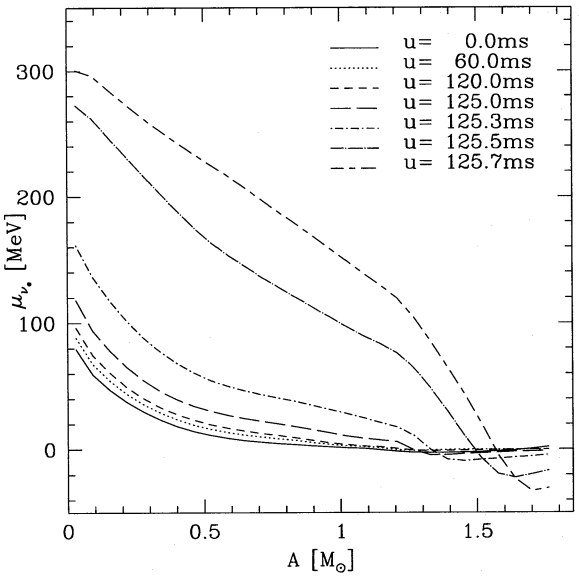

FIG. 7.—Radial profiles of the electron neutrino Fermi energy μ_{ν_e} for different observer times u. In the interior μ_{ν_e} rises continuously with time as the star contracts. In the outer part of the star μ_{ν_e} is kept close to zero at early times by the emission of ν_e and $\bar{\nu}_e$ (see text for details), whereas it drops to significantly negative values during the fast compression in the dynamical collapse.

counterbalanced by an enhanced emission of $\bar{\nu}_e$ relative to ν_e. Preferential loss of electron antineutrinos leads to an increase of Y_e and of the electron chemical potential (Fermi energy) μ_e (Fig. 8), thus driving μ_{ν_e} back to zero. While during the quasi-static phase the changes are slow and the neutrinos can leave the star fast enough to keep μ_{ν_e} near zero, this is not the case any more when the dynamical collapse has set in. The thermodynamical changes in the star proceed very rapidly then, and, moreover, the increasing density and temperature lead to a growth of the neutrino opacity and slow down neutrino diffusion considerably. This is the reason why finally the neutrino chemical potential μ_{ν_e} near the surface can reach increasingly negative values.

During the dynamical collapse the electron neutrino chemical potential climbs to a value near 300 MeV at the center. This value is even higher than the electron chemical potential, which reaches 270 MeV, but whose increase is limited by the formation of hyperons which consumes neutrons and thus constrains the increase of the neutron chemical potential. The region of very strong hyperonization in the deeper parts of the protoneutron star is therefore visible in Figure 8 by a saturation of μ_e and a flattening of its growth toward the center into a plateau with a nearly constant value. For deleptonized (i.e., $\mu_{\nu_e} = 0$) cold matter the saturation value of μ_e is around 200 MeV. Because of the low ν_e chemical potential, this value is indeed realized in our initial model. However, when μ_{ν_e} starts to rise drastically along with the contraction of the star, μ_e also increases.

3.2. *Neutrino Emission*

The evolution of the star is governed by the loss of neutrinos. In Figures 9 and 10 we show the luminosities $e^{2\psi}L_{\nu_i}$ of electron neutrinos ν_e, electron antineutrinos $\bar{\nu}_e$, and the sum of the luminosities of the heavy-lepton neutrinos, $\nu_x = \nu_\mu + \bar{\nu}_\mu + \nu_\tau + \bar{\nu}_\tau$. The factor $e^{2\psi}$ crudely accounts for gravitational redshift and time dilation for an observer at infinity (see BST2). Figure 10 is an expansion of the last 2 ms of the simulation. The three phases of our model, initial relaxation ($u \lesssim 50$ ms), a longer stage of quasi stationarity (50 ms $\lesssim u \lesssim$ 125.0 ms), and the final dynamical collapse ($u \gtrsim 125.0$ ms), can be well identified from the neutrino luminosities.

While the relaxation of the initial model is barely visible in the luminosities of $\bar{\nu}_e$ and ν_x, it is very pronounced for ν_e. The ν_e luminosity starts out at an artificially high flux value which decays within about 50 ms. This is a direct consequence of the thermodynamical and structural adjustment of the initial model, which manifests itself in decreasing

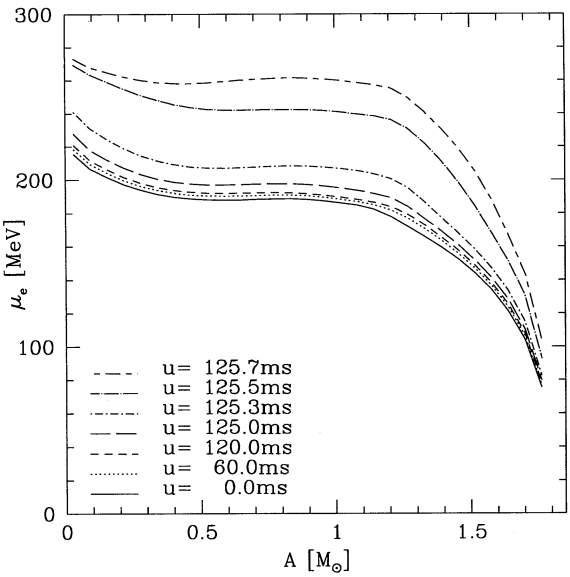

FIG. 8.—Radial profiles of the electron Fermi energy μ_e for different observer times u. μ_e shows a continuous rise with time because the star contracts, but flattens toward the center in the region of strong hyperon production.

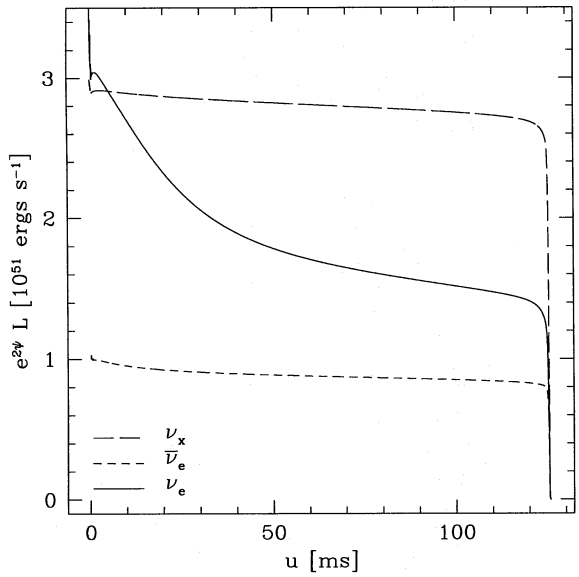

FIG. 9.—Neutrino luminosities "at infinity" as a function of observer time u. The ν_x flux represents the sum of the contributions from all heavy-lepton neutrinos, ν_μ, $\bar{\nu}_\mu$, ν_τ, and $\bar{\nu}_\tau$. The initial relaxation of the protoneutron star model is visible in an excessive ν_e luminosity for $u \lesssim 50$ ms. A phase of quasi-stationary neutrino emission is followed by the suppression of the fluxes in the final gravitational collapse to a black hole.

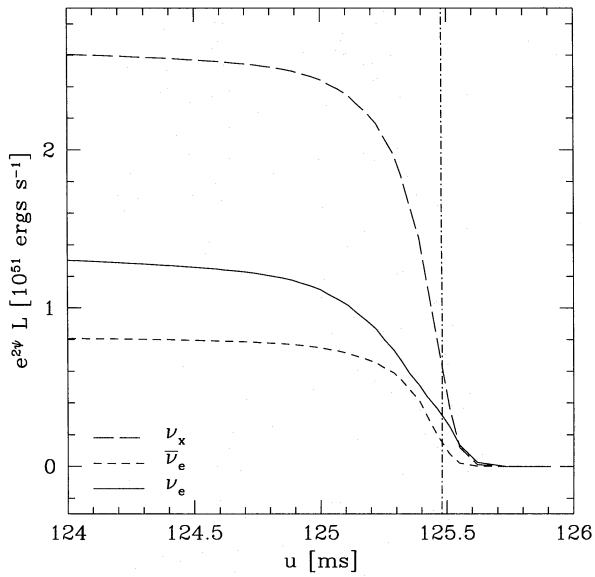

FIG. 10.—Enlargement of the last 2 ms of the evolution shown in Fig. 9. The vertical line marks the time at which the surface of the star crosses the radius $R = 3GM/c^2$. Note that the ν_e luminosity drops less steeply and vanishes later than the fluxes of the other neutrino types.

temperatures (and electron neutrino chemical potentials) in the surface layers (the outermost ~ 0.2–$0.3\ M_\odot$) of the protoneutron star. Because of the large heat capacity of the stellar matter, the excess luminosity of ν_e during the short initial phase can easily be accounted for by very small temperature changes. The thermal energy of a nondegenerate gas of nucleons with a temperature of 1 MeV is about 3×10^{50} ergs per $0.1\ M_\odot$, while an excess luminosity of 2×10^{51} ergs s^{-1} over a period of 50 ms carries away an energy of only 10^{50} ergs. Since in neutronized matter the largest opacities are those for ν_e, their emission is more severely influenced by small surface effects. In contrast, the emission of $\bar{\nu}_e$ and ν_x is more similar to a volume emission with a larger fraction of the radiated neutrinos coming from deeper layers of the star.

After about 50 ms all neutrino fluxes including those of ν_e have achieved quasi-stationary values and decrease on the long timescale of the quasi-static contraction of the protoneutron star. The ν_e luminosity is about $e^{2\psi}L_{\nu_e} \approx 1.4$–$1.6 \times 10^{51}$ ergs s^{-1}, for $\bar{\nu}_e$ we get $e^{2\psi}L_{\bar{\nu}_e} \approx 0.8$–$0.9 \times 10^{51}$ ergs s^{-1}, and for ν_x we find $e^{2\psi}L_{\nu_x} = 4 \times e^{2\psi}L_{\nu_\mu} \approx 2.7$–$2.9 \times 10^{51}$ ergs s^{-1}. These numbers are in very good agreement with the diffusion results of KJ. The higher value of the ν_e luminosity compared to the $\bar{\nu}_e$ luminosity reflects the fact that the star is still in the process of deleptonization, which one naturally expects if the final gravitational instability is instigated by a neutrino-mediated loss of lepton number.

It should be noted that the neutrino luminosities $e^{2\psi}L_{\nu_i}$ computed in the present work are only approximations to the luminosities observed at infinity, because they do not take into account that in a very strong gravitational field tangentially emitted neutrinos are forced onto strongly curved trajectories and thus are delayed in their escape from the star. At late times, tangentially emitted neutrinos describe unstable circular orbits and form a cloud around $R \sim 3GM/c^2$. The luminosity at late times is dominated by neutrinos that eventually leak out from this cloud to infinity rather than being swallowed by the black hole (Ames & Thorne 1968; Shapiro 1989). To calculate the correct luminosity at infinity requires detailed ray-tracing computations in the curved spacetime. The philosophy behind the leakage scheme assumes immediate escape of the emitted neutrinos which is equivalent to assuming that all neutrinos are radiated into the radial direction. Therefore, our luminosities can be considered as approximations to the true luminosities until some time after the moment when the stellar surface crosses the radius $R = 3GM/c^2$ (*vertical dashed-dotted line* in Fig. 10 and in Fig. 12 below), and the effects from the formation of a neutrino cloud must be expected to dominate. At very late times our luminosities will underestimate the true ones because those are still fed by neutrinos that continue to leak out from the neutrino cloud, damped with an exponential time constant of $3^{3/2}GM/c^3$. In contrast, in our numerical treatment the emission is simply chopped off due to increasing gravitational redshift and time dilation.

The luminosities found here differ from the situation in the gravitational collapse of a "cold" ($T \ll 1$ MeV) neutron star. Cold neutron stars are essentially transparent to neutrinos. Therefore, Gourgoulhon & Haensel (1993) found a characteristic rise of the neutrino luminosities due to the compressional heating of the collapsing star. The strong increase of the neutrino emission rates was only truncated when the black hole formed. For the neutrino-opaque situation considered in the present work, a simple dimensional analysis shows that the neutrino flux from a Newtonian star should scale approximately like

$$L_\nu \propto \frac{\epsilon_\nu R_*^3}{t_{\rm diff}} \propto \frac{T^2}{\rho_0^{4/3}} \frac{[\mathscr{F}_3(\eta_\nu)]^2}{\mathscr{F}_5(\eta_\nu)} . \tag{7}$$

Here $\epsilon_\nu \propto T^4 \mathscr{F}_3(\eta_\nu)$ is the neutrino energy density with $\mathscr{F}_n(y) = \int_0^\infty dx x^n/(1 + e^{x-y})$ being the Fermi integral for relativistic particles, $t_{\rm diff} \propto R_*^2 \langle\kappa\rangle$ is the neutrino diffusion timescale with $\langle\kappa\rangle \propto \rho_0 T^2 \mathscr{F}_5(\eta_\nu)/\mathscr{F}_3(\eta_\nu)$ representing the neutrino opacity averaged over a thermal neutrino spectrum when fermion-blocking effects are disregarded, and $R_* \propto (M_*/\rho_0)^{1/3}$ relates stellar mass M_*, stellar radius R_*, and (average) density ρ_0. For nondegenerate neutrinos, $\mu_\nu = \eta_\nu T \lesssim 0$, one finds $L_\nu^{\rm nd} \propto T^2/\rho_0^{4/3}$, while for the less relevant case of extremely degenerate neutrinos one obtains $n_\nu \propto \rho_0 Y_\nu \propto \mu_\nu^3$ and $L_\nu^{\rm d} \propto (Y_\nu/\rho_0)^{2/3}$ [replace $T^{n+1}\mathscr{F}_n(\eta_\nu)$ in equation (7) by its limit $\mu_\nu^{n+1}/(n+1)$ for $T \to 0$]. With the density and temperature histories of Figures 4 and 5, respectively, these relations suggest a slow decline of the neutrino fluxes with time.

Similar, straightforward arguments predict for the Newtonian case an increase of the average energy of neutrinos emitted by the star roughly proportional to the temperature in the star,

$$\langle\epsilon_\nu\rangle \propto T \frac{[\mathscr{F}_3(\eta_\nu)]^2 \mathscr{F}_4(\eta_\nu)}{[\mathscr{F}_2(\eta_\nu)]^2 \mathscr{F}_5(\eta_\nu)} . \tag{8}$$

This, however, has to be interpreted with great caution because $\langle\epsilon_\nu\rangle$ depends more sensitively than the total neutrino luminosity on differential effects rather than simply on global changes of density and thermodynamical parameters in the star; increasing T and ρ_0 lead to higher neutrino opacities, and thus reduce the fraction of the neutrinos that is emitted from the very hot core relative to the part of the flux that originates from the cooler, outer regions. There-

fore, one must expect $\langle \epsilon_\nu \rangle$ to increase more slowly than the stellar temperature T. Yet, we shall see below that the discussed effect has visible implications for the properties of the ν_e emission.

During the dynamical stage of the collapse, when more and more matter approaches the event horizon, gravitational effects have a strong influence on the neutrino signal. Initially, this affects the $\bar{\nu}_e$ and ν_x luminosities more strongly than the ν_e emission, because a larger contribution to the $\bar{\nu}_e$ and ν_x emission comes from deeper layers and is more strongly redshifted on the average. The electron neutrinos with their higher optical depths in neutronized matter are radiated to a larger fraction from a region close to the surface, where the relative increase of the redshift is slower (Fig. 2). Therefore, the drop of the ν_e luminosity appears less steep at times $u \gtrsim 125.2$ ms.

This tendency is also present in the average energies of the emitted neutrinos $e^{\psi}\langle \epsilon_{\nu_i} \rangle$ (for an observer at infinity), as can be verified in Figures 11 and 12, the latter figure showing again an enlargement of the last 2 ms of our calculation. In Figure 12 one can see that $e^{\psi}\langle \epsilon_{\nu_e} \rangle$ does not only drop later than $e^{\psi}\langle \epsilon_{\bar{\nu}_e} \rangle$ and $e^{\psi}\langle \epsilon_{\nu_x} \rangle$ when the gravitational redshift and the opacities rise during the collapse, but it even has a short phase of noticeable *increase* at $u \approx 125.4$ ms (see the discussion in connection with equation [8]). Finally, however, the redshift dominates, and $e^{\psi}\langle \epsilon_{\nu_e} \rangle$ is also suppressed.

These differences can again be explained by the fact that a larger part of the ν_e flux is emitted from layers near the surface. The suppressing effects of redshift and opacity increase are overcompensated in case of ν_e by the monotonic rise of the temperatures in the whole star, in particular in the surface regions, for $u \gtrsim 50$ ms (Fig. 5). Note that the change of $e^{\psi}\langle \epsilon_{\nu_e} \rangle$ due to the temperature increase is also not outdone by the effects of the drop of μ_{ν_e} to considerably negative values in the outer regions of the star during the dynamical collapse ($u \gtrsim 125.0$ ms). The shift from chemical potential values near zero to $\mu_{\nu_e} < 0$ has only a marginal influence on the neutrino distributions at local thermal equilibrium and on the thermally averaged ν_e opacity.

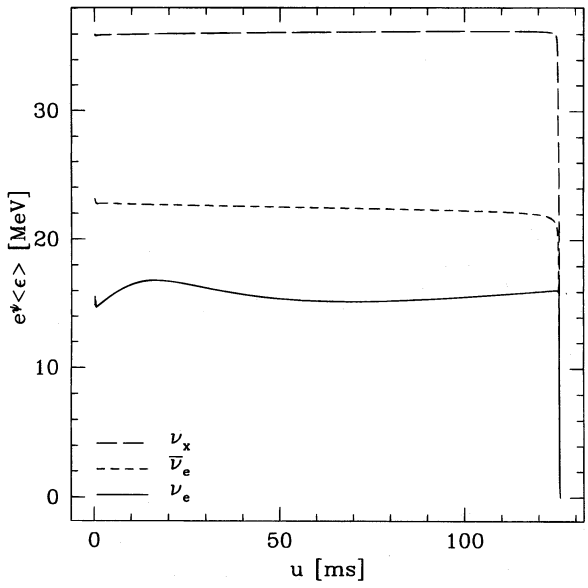

FIG. 11.—Average energies of the emitted neutrinos vs. time u for an observer at infinity. After the initial relaxation phase ($u \lesssim 50$ ms) the mean energy of ν_e shows a monotonic, slow increase, whereas $e^{\psi}\langle \epsilon_{\bar{\nu}_e} \rangle$ decreases slightly and $e^{\psi}\langle \epsilon_{\nu_x} \rangle$ stays nearly constant.

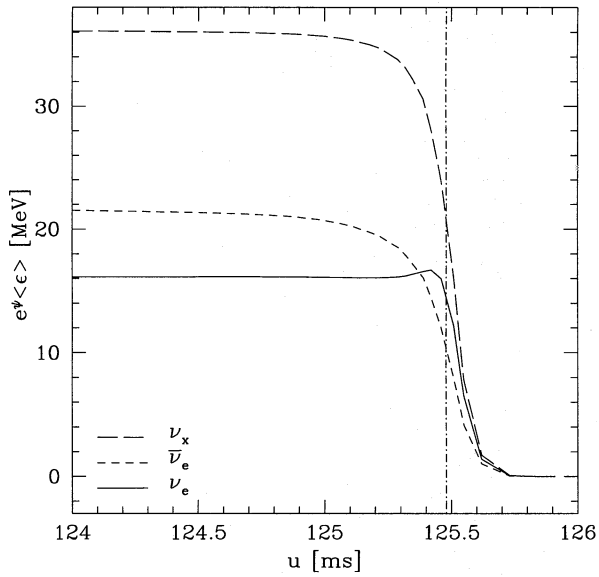

FIG. 12.—Enlargement of the last 2 ms of the evolution shown in Fig. 11. The vertical line marks the time at which the surface of the star crosses the radius $R = 3GM/c^2$. While $e^{\psi}\langle \epsilon_{\bar{\nu}_e} \rangle$ and $e^{\psi}\langle \epsilon_{\nu_x} \rangle$ are quickly suppressed by the increasing gravitational redshift during the dynamical collapse, $e^{\psi}\langle \epsilon_{\nu_e} \rangle$ first rises and becomes even larger than $e^{\psi}\langle \epsilon_{\bar{\nu}_e} \rangle$ before finally dropping off.

The mean energies seen by an observer at infinity as given in Figures 11 and 12 may be somewhat too high because the surface region of the stellar model is poorly represented by the use of only 30 radial zones, which, e.g., implies an underestimation of the optical depths. However, the relative sizes of $e^{\psi}\langle \epsilon_{\nu_i} \rangle$ for the different neutrino types very nicely match with results from more elaborate treatments of neutrino transport during protoneutron star cooling. The good overall agreement with diffusion calculations makes us confident that the evolutionary trends of the neutrino fluxes and mean energies in our simulations are not an artifact of our simplifications. Instead, we believe that these trends are typical of the collapse of hot neutron stars to black holes.

4. SUMMARY

We have investigated the collapse of hot, newly formed neutron stars to black holes. In the adopted scenario the gravitational instability is caused by a phase transition and softening of the EOS that is associated with the formation of additional hadronic degrees of freedom besides neutrons and protons in the supranuclear medium. Because the creation of new hadronic states is favored by a high neutron abundance and degeneracy, the maximum stable mass of a deleptonized neutron star is lower than the limiting mass of the lepton-rich configuration. The hyperonic EOS used in the present work allows lepton-rich protoneutron stars in the mass window $1.58\ M_\odot \lesssim M \lesssim 1.77\ M_\odot$ (gravitational mass) to be stable for the lepton-loss timescale of several seconds after their birth in the core collapse of a massive star. This intermediate phase of stability is sufficiently long that neutrinos from the protoneutron star can deposit enough energy in the surrounding matter of the progenitor star to cause a Type II supernova explosion. The lepton number and energy loss through the emission of neutrinos drives the protoneutron star's evolution toward the final

gravitational instability which sets in when the ongoing deleptonization decreases the limiting mass below the actual gravitational mass of the star.

In this paper we concentrate on the last phase of the quasi-static evolution, simulate the onset of the final gravitational instability, and follow the dynamical infall to its completion, i.e., until the moment when the stellar surface approaches the event horizon. In our adopted time slicing the subsequent collapse appears frozen, and the radial profiles of hydrodynamical quantities and thermodynamical parameters essentially do not change any more. For an observer at infinity the dynamical collapse takes only about 1 ms and converges to an apparent state where the central density of the star is close to 4×10^{15} g cm^{-3}, the central temperature near 100 MeV, and the surface velocity about 0.5c. At the same time the luminosities drop to vanishingly small values so that the star disappears from the view of a distant observer.

The size and temporal decline of the neutrino fluxes during the quasi-static period as computed with the elaborate leakage scheme of this work are in very good agreement with the diffusion results of KJ. Moreover, we can also confirm excellent qualitative agreement with the temporal behavior of the dynamical collapse phase obtained by BST2 who employed a simple relativistic diffusion approximation of the neutrino transport. Also, BST2 used a kaon-condensate EOS in their simulations as opposed to the hyperonic EOS in this work, which suggests that the principal features of the stellar implosion hardly depend on the details of the supranuclear EOS. In particular, the central densities and central temperatures of the stars are very similar in both models at the time when the evolution gets frozen in for an external observer.

The characteristics of the neutrino emission are distinctively different from the case of a collapsing cold neutron star. The latter is essentially transparent to neutrinos. When the collapse sets in, the increasing densities, temperatures, and neutrino production rates therefore cause a temporary luminosity maximum before the neutrino fluxes are finally terminated when the black hole forms (Gourgoulhon & Haensel 1993). In contrast, a hot neutron star is opaque to neutrinos, and our model does not show a late, luminous outburst or catastrophic increase of the neutrino emission. Instead, when the contraction of the star accelerates and becomes dynamical, the neutrino luminosities are gradually suppressed below their quasi-stationary, slowly decaying values during the Kelvin-Helmholtz cooling phase.

Our results reveal differences in the late-time behavior of the neutrino fluxes and mean neutrino energies that indicate an unequal effect of a strong gravity field on the emission of different neutrino types as seen by an observer at infinity. The $\bar{\nu}_e$ and ν_x luminosities decay more steeply than the ν_e flux because $\bar{\nu}_e$ and ν_x originate, on the average, from deeper regions of the star where the lapse function e^{ψ} decreases faster and more strongly at the onset of the gravitational instability. Because ν_e decouple from layers closer to the surface, their gravitational redshift is less extreme and the observable mean ν_e energies even rise slightly, which reflects the overall compressional heating of the star. During the last dynamical phase of the collapse the average energy of ν_e exceeds that of $\bar{\nu}_e$. This means an inversion of the usual hierarchy of the mean spectral energies which are typically higher for $\bar{\nu}_e$ than for ν_e. In the very late stages of the collapse the gravitational effects are so dominant that the observable ν_e flux becomes as luminous and energetic as the combined emission of heavy-lepton neutrinos ν_μ, $\bar{\nu}_\mu$, ν_τ, and $\bar{\nu}_\tau$.

These findings have more general implications that might reach beyond the specific context of the dynamical scenario discussed in the present work. They indicate that the predicted characteristics of the neutrino signal, in particular the luminosities and spectra of different neutrino types in comparison with each other, are sensitive to the relative strength of the gravitational field near the center and the surface of the neutrino-radiating compact object. Gravitational redshift and time dilation effects may distort the standard picture of approximately equal luminosities for all neutrino types, ν_e, $\bar{\nu}_e$, ν_μ, $\bar{\nu}_\mu$, ν_τ, and $\bar{\nu}_\tau$, and may change the usual order of mean neutrino energies which assumes muon and tau neutrinos to be more energetic than $\bar{\nu}_e$, and these more energetic than ν_e. This can be important for massive protoneutron stars if the stars become very compact due to the particular properties of the supranuclear EOS.

We are very grateful to N. K. Glendenning for providing us with the table of his equation of state. H. T. J. would like to thank Y.-Z. Qian and S. Woosley for interesting discussions. This work was supported in part by NSF Grants AST 91-19475, AST 92-17969, and PHY 94-08378, and by NASA Grants NAGW-2364 and NAG 5-2081. T. W. B. gratefully acknowledges support by a fellowship of the German Academic Exchange Service (DAAD), H. T. J. by an Otto Hahn postdoctoral scholarship of the Max-Planck-Society.

REFERENCES

Alexeyev, E. N., et. al. 1987, Phys. Lett., B205, 209 (Baksan Collaboration)
Ames, W. L., & Thorne, K. S. 1968, ApJ, 151, 659
Baumgarte, T. W., Shapiro, S. L., & Teukolsky, S. A. 1995, ApJ, 443, 717 (BST1)
———. 1996, ApJ, 458, 680 (BST2)
Bionta, R. M., et. al. 1987, Phys. Rev. Lett., 58, 1494 (IMB Collaboration)
Brown, G. E., & Bethe, H. A. 1994, ApJ, 423, 659
Brown, G. E., Bruenn, S. W., & Wheeler, J. C. 1992, Comments Astrophys., 16, 153
Brown, G. E., & Weingartner, J. C. 1994, ApJ, 436, 843
Burrows, A. 1988, ApJ, 334, 891
Chen, K., & Colgate, S. 1995, preprint LAUR-95-2972, Los Alamos
Colpi, M., Shapiro, S. L., & Wasserman, I. 1995, Cornell Univ., preprint CRSR 1103
Fryer, C. H., Benz, W., & Herant, M. 1996, ApJ, 460, 801
Glendenning, N. K. 1985, ApJ, 293, 470
———. 1989, in The Nuclear Equation of State, Part A, ed. W. Greiner & H. Stöcker (New York: Plenum), 751
———. 1995, ApJ, 448, 797
Gourgoulhon, E., & Haensel, P. 1993, A&A, 271, 187
Hernandez, W. C., & Misner, C. W. 1966, ApJ, 143, 452
Hirata, K., et. al. 1987, Phys. Rev. Lett., 58, 1490 (Kamiodande II collaboration)
Janka, H.-Th. 1995, in Astro-Particle-Physics (SFB 375), Proc. 1995 March 6–10 workshop in Ringberg Castle, Tegernsee, Germany, ed. A. Weiss, G. Raffelt, W. Hillebrandt, & F. von Feilitzsch, (Munich: Technische Universität), 154 (astro-ph/9505034)
Keil, W., & Janka, H.-Th. 1995, A&A, 296, 145 (KJ)
Mayle, R.W., Tavani, M., & Wilson, J. R. 1993, ApJ 418, 398
Percival, J. W., et. al. 1995, ApJ, 446, 832
Ruffert, M., Janka, H.-Th., & Schäfer, G. 1996, A&A, in press
Shapiro, S. L. 1989, Phys. Rev. D, 40, 1858
Shelton, I. 1987, IAU Circ. 4316
Takahara, M., Takatsuka, T., & Sato, K. 1991, Prog. Theor. Phys., 86, 57
Takatsuka, T. 1992, in The Structure and Evolution of Neutron Stars, ed. D. Pines, R. Tamagaki, & R. Tsuruta (New York: Addison-Wesley), 257
Thorsson, V., Prakash, M., & Lattimer, J. M. 1994, Nucl. Phys., A572, 693
Woosley, S. E., & Weaver, T.A. 1995, ApJS, 101, 181